Raman scattering from MeV-ion implanted diamond

J. D. Hunn, S. P. Withrow, and C. W. White
Oak Ridge National Laboratory, Oak Ridge, Tennessee 37831

D. M. Hembree, Jr.
Oak Ridge Y-12 Plant, Oak Ridge, Tennessee 37831

(Received 2 March 1995)

Single-crystal diamond has been irradiated with 4-MeV carbon ions to doses in the range $(0.5-130)\times10^{16}$ ions/cm^2. With increasing implantation damage, the triply degenerate one-phonon Raman mode at 1332 cm^{-1} broadens and shifts down to around 1300 cm^{-1}. This corresponds to a broad peak in the one-phonon density of states predicted for Raman scattering from an amorphous sp^3 carbon network. Additional Raman peaks appear at 1451, 1498, and 1634 cm^{-1}. These do not correspond to any previously observed peaks in carbon materials and may be unique to implantation above 1 MeV. These three peaks, together with the Raman scattering below 1300 cm^{-1}, correspond well with the density of states of an amorphous carbon network of mostly fourfold bonded carbon with some localized threefold bonding.

I. INTRODUCTION

The sharp, characteristic peaks observed in Raman-scattering spectra from single-crystal materials are due to the periodicity of the lattice, which gives rise to a set of momentum selection rules. For example, one phonon scattering in single-crystal diamond is dominated by a single intense peak at 1332 cm^{-1}, with a width of a few wave numbers. Even in a noninfinite, imperfect crystal, if the periodicity of the lattice extends over a distance large compared to the wavelength of the scattered light, then the selection rules still apply and sharp Raman features are observed. In a highly disordered material, however, the loss of long-range order results in the absence of a well-defined crystal momentum and a breakdown of the wave-vector selection rules. Under these conditions a range of light-scattering processes is allowed.

In an amorphous material, all the vibrational modes can contribute to the optical scattering. For this case the first-order Raman-scattering spectrum is related to the vibrational density of states weighted by mode coupling constants. If the weighting factor for all the scattering modes is assumed to be constant, then the reduced Raman intensity $I_R(\omega)$ defined as

$$I_R(\omega)=I(\omega)/\{[1+n(\omega,T)]/\omega\} \ , \qquad (1)$$

replicates the density of states (DOS).[1] In Eq. (1), ω is the frequency shift relative to the excitation frequency, $I(\omega)$ is the measured Stokes contribution to Raman scattering, and $n(\omega,T)$ is the Bose-Einstein distribution $[\exp(\hbar\omega/kT)-1]^{-1}$. A comparison of $I_R(\omega)$ for the amorphous semiconductors Si and Ge with their respective densities of states shows a qualitative match for peak shape and position.[2-4] A quantitative match of the relative intensities of the peaks is not expected, because the Raman-scattering cross section for all the modes is not constant.

Success in applying Eq. (1) to carbon has not been reported. Raman spectra from amorphous carbon (*a*-C) films show a wide range of variation with regard to peak positions, linewidths, and line shapes. Typically such spectra have their strongest Raman yield above 1400 cm^{-1}. Attempts to match these spectra to the density of states of sp^3-bonded carbon, which has a cutoff around the wave number of the one phonon line at 1332 cm^{-1}, have been unsuccessful. Even allowing for some percentage of sp^2-bonding to be present in the films has not achieved a reasonable match.[5,6] Sputtered *a*-C films, expected to contain predominantly threefold bonded carbon, show a closer match to the DOS of crystalline graphite.[7] Laser assisted or arc deposited *a*-C films are estimated to contain up to 75% fourfold "diamondlike" bonding, due to the higher energy of the deposited species. The higher sp^3 ratio in these films results in more Raman scattering below 1100 cm^{-1} than in rf-sputtered films.[8] However, the Raman spectra is still dominated by a strong, broad peak around 1550 cm^{-1}, identified as an sp^2-stretching mode in graphite. Raman spectra have also been reported on diamond damaged using ion implantation with carbon at 150 keV (Ref. 9) and Ar at 1 MeV.[10] In both of these studies, implantation resulted in the complete loss of the Raman spectrum characteristic of crystalline diamond and the concurrent appearance of a broadband peaked around 1550 cm^{-1}, similar to that observed in some *a*-C films that could be fit with Raman peaks known to be related to graphite or disordered graphite.

Ion implantation is ideally suited as a method to introduce controlled amounts of damage into a single-crystal material and at high doses a crystalline material can even be turned amorphous in the near surface region. Ion implantation of a single-crystal material produces lattice defects, due to the transfer of energy governed by two main processes, electronic and nuclear stopping.[11] At high velocities, most of the ion energy loss is due to electronic stopping, which does not directly introduce appreciable

 ©1995 The American Physical Society

damage in the crystal. As the ion energy (and velocity) decreases near the end of range (corresponding to increasing penetration depth), nuclear energy losses increase dramatically. This is illustrated in Fig. 1 by a TRIM (Ref. 12) simulation for 4-MeV carbon ions incident on diamond. The exchange of energy through nuclear collisions generates atomic displacements. Therefore, at the peak of the nuclear energy loss, a high concentration of lattice point defects is created. In contrast, in the material above this region, where electronic stopping is the dominant energy-loss process, less lattice damage is introduced. However, it is evident that lattice defects are present in the "electronic stopping" region nearer the surface, since when this layer is removed from the substrate[13] it exhibits a slight yellow coloration, which is caused by optical absorption at lattice vacancies.[14]

In the present work, ion implantation of 4-MeV carbon into single-crystal diamond has been used to create damage in the near surface region of the diamond substrate. Raman scattering and Rutherford backscattering (RBS) spectroscopies are used to study damage production and changes in the diamond morphology as a function of dose.

II. EXPERIMENT

The samples used in this study were IIa diamond single-crystal square windows ($0.25\times3.0\times3.0$ mm) with [100], [110], and [111] orientations. They were polished to < 10-nm surface roughness and oriented to within 3° of normal. Raman spectra of the virgin crystals show a single one-phonon peak at 1332 cm^{-1} with a typical linewidth of 2.7 cm^{-1}. Rutherford backscattering/channeling (RBS/C) with 1.5-MeV protons gives a χ_{min} of 3% for the virgin crystals. (χ_{min} is defined in the usual way as the ratio of the backscattered yield with the beam oriented along a major crystallographic direction to the yield with the beam oriented along a random direction. This value for χ_{min} indicates good crystal quality with few defects in the virgin crystal.)

For ion implantation, a 1.7-MV Tandem was used to accelerate doubly charged carbon ions to a particle energy of 4 MeV. The carbon beam was scanned over a half inch aperture to give a uniform implant profile. Crystals of all three orientations were implanted in steps of 0.5×10^{16} cm^{-2}, up to a dose of 5.0×10^{16} cm^{-2} and in larger steps up to a dose of 130×10^{16} cm^{-2}. The samples were implanted at least 2° off axis in order to prevent channeling of the implanted ions and were held at -196 °C to limit thermal diffusion and the production of extended defect structures.

The samples were characterized using Raman spectroscopy and Rutherford backscattering/channeling. Raman spectra were taken using the 488- and 514.5-nm lines from an Innova 90-5 argon-ion laser. A $100\times$ Leitz objective with a numerical aperture of 0.9 was used for micro-Raman with a typical laser input power of 100 mW. The diameter of the focal point of the beam was approximately 2 μm. Spectra were obtained for a 500–1800-cm^{-1} Raman shift and fit with a Breit-Wigner line shape as described below. A 1.5-MeV proton beam was used for the RBS/C. The beam was focused and collimated to a 1-mm spot. Backscattered protons were collected in a silicon barrier detector positioned at 120° relative to the direction of the incident beam.

III. RESULTS AND DISCUSSION

Rutherford backscattering/channeling spectra from [100] diamond implanted at several doses with 4-MeV carbon ions are given in Fig. 2. The spectra have been normalized by dividing the yield in the channeled direction by the yield from a random spectrum. Damage to the lattice as a result of ion implantation is detected by an increase in channeling yield compared to that from a virgin crystal. The accumulation of lattice damage with increasing dose is shown by the successively higher backscattered yield. At a fixed dose, lattice damage also increases with increasing depth up to the end of range of

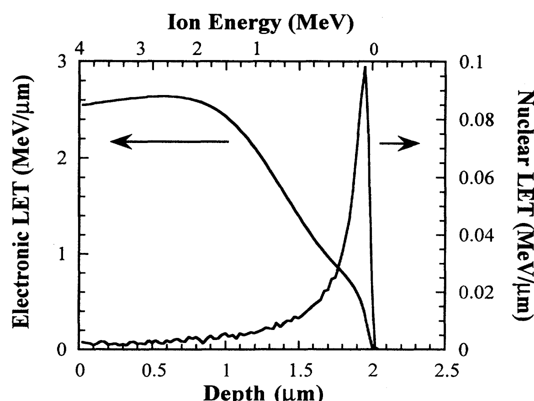

FIG. 1. TRIM simulation of 4-MeV carbon ions incident on diamond. Lattice damage correlates with the nuclear damage energy.

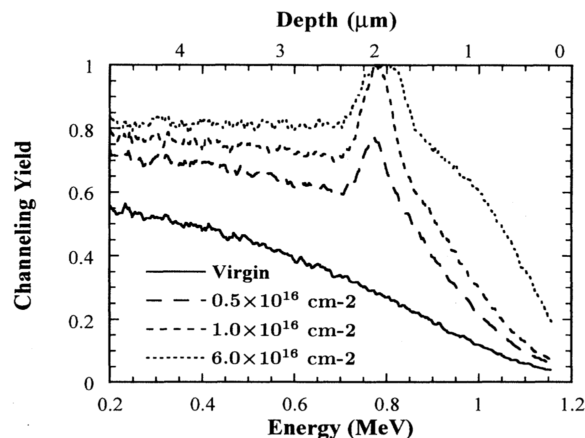

FIG. 2. RBS/channeling spectra of [100] diamond implanted with 4-MeV carbon ions. The ion dose used in each case is indicated. The channeling yield is obtained by dividing each aligned spectrum by a random spectrum. A yield of unity means no channeling.

the ion, roughly 2 μm, where a peak is seen in the damage density as predicted by the TRIM simulation in Fig. 1. The heavily damaged region at the end of range becomes opaque for a dose of 1×10^{16}, approximately when the RBS/C yield reaches the random level. Similar spectra were obtained for the [110] and [111] orientations. The [111] was found to damage most easily, followed by the [100] and then the [110].[15] This effect may be due to partial channeling of the implanted ions. A similar orientation dependence for damage accumulation was seen in TRIM simulations of MeV channeling along these three axial directions.[16]

Figure 3 shows reduced Raman spectra from a [100] sample implanted with carbon ions at 4 MeV. The data were obtained as a function of implantation dose, using an excitation wavelength of 488 nm. Five peaks are labeled in Fig. 3(b): a broadband between $\sim$600–800 and sharper structures at 1332, 1451, 1498, and 1634 cm^{-1}. These peaks are not dependent on the implant species; high-energy carbon or oxygen implantation yielded the same Raman features. In Fig. 3(b), some contribution of the 1332-cm^{-1} signal may originate from the underlying undamaged crystal. The sampled depth depends on photon absorption. The absorption coefficient in IIa diamond at 488 nm is 4.4 cm^{-1}. At doses below approximately 1.0×10^{16}, before the sample becomes opaque, Raman scattering originates both from the damaged layer at the surface as well as from undamaged single-crystal diamond below the implant. At higher doses, the excitation laser light is absorbed in the opaque layer and only the implanted surface layer of the diamond is sampled by the Raman analysis.

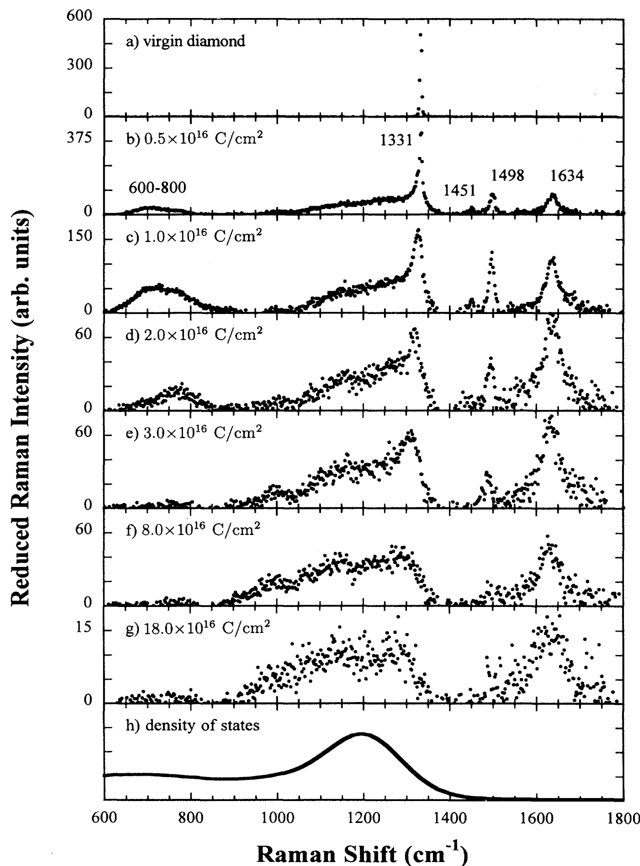

FIG. 3. (a)–(g) Reduced Raman spectra from a [100] diamond successively implanted to increasing doses with 4-MeV carbon ions. A linear background subtraction has been made on the raw spectra. (h) Approximate one-phonon density of states for sp^3 amorphous carbon.

The broadband between 600–800 cm^{-1} (502–507 nm) does not appear with excitation at 514 nm and hence can be identified as a photoluminescence (PL) band. It is only observed at the lowest implant doses, initially increasing with dose up to around 1.0×10^{16} and then decreasing. The PL band can be separated into two peaks: one centered around 670 cm^{-1}, possibly from the defects previously identified in diamond[14] and a second at $\sim$750 cm^{-1}. At a dose of 2.0×10^{15} (not shown in Fig. 3) the 670 peak is dominant, while at 2.0×10^{16} the 750-cm^{-1} peak persists and the 670 peak has all but disappeared. The photoluminescence band is also observed for low-dose carbon implantation at 100 keV, hence is not dependent on MeV implantation energies.

The remaining four spectral features labeled in Fig. 3(b) are due to Raman scattering. Peak positions were determined using a Breit-Wigner-Fano line shape[17] with a linear background subtraction,

$$I_R(\omega) = I_0\left[1+\frac{\omega-\omega_0}{q\Gamma}\right]^2 \Bigg/ \left[1+\left[\frac{\omega-\omega_0}{\Gamma}\right]^2\right] + (a+b\omega)\,, \tag{2}$$

where $I_R(\omega)$ is the reduced Raman intensity, I_0 is the peak height, ω_0 is the excitation frequency, q^{-1} is the skewness factor, and Γ is the linewidth. This line shape provides a better fit to the data than a straight Lorentzian ($q^{-1}=0$). Peak fits were made on thirty-seven separate spectra obtained from samples of all three orientations studied following 4-MeV carbon implantation. Results are qualitatively similar on all three faces.

The 1332-cm^{-1} triply degenerate one-phonon diamond peak is the only Raman line observed in the virgin samples. As Fig. 3 shows, this feature rapidly decreases in intensity and broadens with increasing ion dose. Concurrently a broadband below 1332 cm^{-1} develops. Above a dose of approximately 3.0×10^{16} the crystalline diamond peak can no longer be clearly resolved from the broadband.

The three Raman peaks above 1332 cm^{-1} in Fig. 3(b), which are not seen in virgin diamond, increase in intensity up to a dose of 1.0×10^{16} ions/cm^2. For higher fluences, they show a general trend of broadening and decreasing in intensity with increasing dose. The peaks at 1451 and 1498 cm^{-1} can no longer be resolved from the background above 10×10^{16} ions/cm^2. However, the peak at 1634 cm^{-1} persists to the highest dose studied at the same relative intensity as the broadband below 1332 cm^{-1}. The peak at 1451 cm^{-1} moves down in wave number with increasing dose (to $\sim$1449 cm^{-1} at a dose

of 2.5×10^{16} cm^{-2}); in contrast, the peaks at 1498 cm^{-1} and 1634 cm^{-1} stay at the same wave number. The overall drop in intensity with increasing fluence can be explained by a decrease in sampling depth, as the front edge of the opaque layer moves toward the diamond surface.

To our knowledge, the three Raman peaks observed here above the 1332-cm^{-1} diamond line have not been observed in other carbonaceous materials and appear to be unique to high-energy implantation into diamond. Spectra obtained following implantation of 1.0×10^{16} carbon ions/cm^2 at 500 keV, 1 MeV, and 4 MeV are compared in Fig. 4. Implantation at 500 keV yields a broad, weak scattering band between 1400 and 1700 cm^{-1}, characteristic of sp^2-bonded carbon. The sharpness and position of the diamond 1332-cm^{-1} line suggests that it originates below the implant region. Above 1 MeV, features around 1495 and 1634 cm^{-1} appear. Previous work on low-dose carbon implantation in diamond at 150 keV did not see these three peaks, but rather only a very broad graphitelike Raman signal at $\sim$1580 cm^{-1} as in the 500-keV sample.[9]

It is also interesting to note in Fig. 3 the absence of any Raman modes known to be related to graphite or sp^2 bonded carbon, even at the highest fluences. Graphite, amorphous carbon, and diamondlike carbon all produce broad scattering bands in the region between 1350–1600 cm^{-1}. Crystalline graphite has a very strong Raman band (called the *G*-band) centered at $\sim$1580 cm^{-1}. The relative scattering efficiency for this band is $\sim$50 times higher than for the 1332-cm^{-1} diamond mode.[18] Hence, Raman, is hypersensitive to graphite in diamond and small amounts of graphite can be detected. The absence of the graphite *G* band and also the disordered graphite *D* band at $\sim$1360 cm^{-1} in the spectra in Fig. 3 shows that there is little if any graphite in the sample.

Ion implantation introduces damage by randomly displacing atoms from their crystal lattice sites. This changes the local bonding structure and results in the loss of long-range order. As the lattice correlation length gets

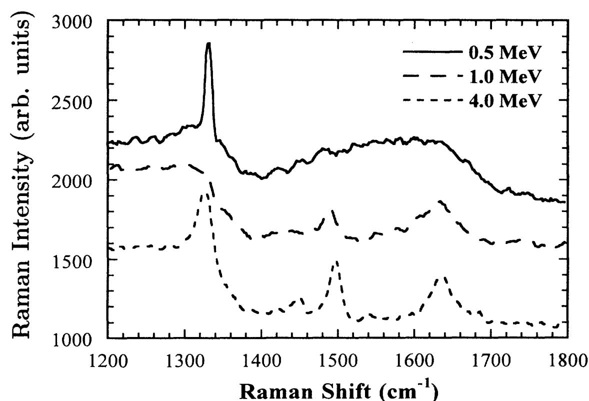

FIG. 4. Raman scattering from single-crystal type-IIa diamond implanted with 1.0×10^{16} carbon ions/cm^2 at three different energies. Vertical scale has been adjusted to overlay the spectra.

shorter, the implanted diamond should scatter light more and more like amorphous carbon. Therefore, one would expect the reduced Raman spectra to approach the density of states of the amorphous material. Because the short-range order is similar and vibrational modes are mostly determined by nearest-neighbor interactions, the one-phonon DOS of amorphous sp^3 carbon can be approximated from that of diamond. Figure 3(h) shows the Gaussian broadened one phonon DOS of diamond calculated with a Gaussian width of 100 cm^{-1}. The broadening is to account for small variations in the bond length and angle in the amorphous state. In Fig. 3, the reduced Raman yield below 1332 cm^{-1} is seen to approach with increasing dose the one-phonon density of states of sp^3 amorphous carbon. This suggests the formation of an amorphous carbon network with fourfold coordinated (diamondlike) bonds at high dose.

However, comparison of the reduced Raman spectra in Fig. 3 to the density of states of a purely sp^3 amorphous carbon does not account for the relatively strong peak at 1634 cm^{-1} or the smaller peaks at 1451 and 1498 cm^{-1}. In fact, one-phonon scattering processes from a sample with diamondlike bonding will not result in scattering at wave numbers higher than those that occur in the DOS. Hence these structures cannot arise from a morphology of only amorphous, sp^3-bonded material. Additional bonding arrangements are required. Recently, a tight binding molecular-dynamics (TBMD) simulation[6] for the DOS of an amorphous carbon consisting of 74% fourfold (sp^3) and 26% threefold (sp^2) bonded atoms has been reported that provides a striking match to the spectrum shown in Fig. 3(g). The simulation was for a liquid carbon quenched under high density. This closely resembles processes expected to occur in the ion track during carbon implantation. In the TBMD simulation, a broad peak below 1400 cm^{-1} was found that is similar to that in the DOS of 100% sp^3 amorphous carbon and is mostly due to extended fourfold bonding. A peak appears in the simulation between 1600 and 1700 cm^{-1} with approximately the same width as our 1634 peak; this peak was identified in the model as stemming from localized threefold bonding. The observed peaks at 1451 and 1498 cm^{-1} are surprisingly sharp to be caused by an essentially amorphizing process such as ion implantation. It is likely that these peaks result from scattering from some localized bonding structure created as the crystal is damaged by the ion beam. Indeed, in the TBMD model, some structure is observed between 1400 and 1600 cm^{-1}, which was attributed to localized bonding between threefold and fourfold coordinated carbon atoms. In the TBMD simulation the threefold and fourfold bonded atoms had a tendency to cluster. This may explain why the 1451- and 1498-cm^{-1} peaks disappeared at higher implantation fluences.

The observed peaks in the Raman spectra between 1400 and 1700 cm^{-1} are unique to high-energy implantation. A plausible explanation for the appearance of these peaks is the effect of internal pressure on the formation of different bonding structures. Implantation at 4 MeV introduces a high concentration of point defects at the end of range, approximately two micrometers below the sur-

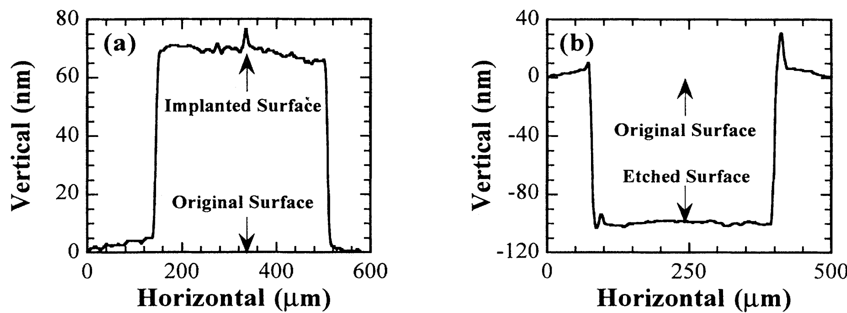

FIG. 5. (a) Vertical expansion caused by implantation of 3.0×10^{16} boron ions/cm^2 at 54 keV. (b) Etch pit after removal of damaged region from the sample in (a).

face (Fig. 1). The stiff, lightly damaged, overlying diamond layer acts to constrain expansion, thus preventing a reduction of density in the heavily damaged, end of range region. Diamond has a density of 3.5 g/cm^3 whereas wholly and partially sp^2-bonded carbons have significantly lower densities (e.g., graphite has a density of 2.25 g/cm^3). For these MeV energy implants, it is probable that a high sp^3/sp^2 ratio is maintained due to the constraint of high density. This is the same constraint that produced the high sp^3 concentration in the TBMD calculations.[6] For implants where the highly damaged end of range occurs closer to the surface, as in the 500-keV implant, the expansion constraint is decreased resulting in higher percentages of sp^2 carbon.

Expansion of the damage region has been observed for low-energy implantation. Figure 5(a) shows the cross-sectional profile of a circular spot on a diamond substrate implanted with 3.0×10^{16} boron ions/cm^2 at 54 keV. The 700 Å of vertical expansion is due to a change in density of the material in the implanted area. Because the material surrounding the implanted spot was undamaged diamond, the expansion was constrained to the vertical direction. Figure 5(b) shows the pit obtained after the implanted carbon was removed by a selective etch.[13] The etch pit defines the volume that expanded, due to the implantation. The sample exhibited a density reduction in the implanted region; this reduction is approximately the difference in density between diamond and graphite. For boron implants at this energy, the end of range is only 1000 Å below the surface and there is little constraint to expansion of the implant region toward the surface. In contrast to these low-energy results, samples implanted at 5 MeV with boron or carbon, where there is a 2-μm constraining overlayer, do not show vertical expansion. In addition, optical absorption studies of the latter samples show enhanced thermal annealing of the implantation damage, due to high internal pressure.[19]

IV. CONCLUSIONS

A Raman study has been made of single-crystal diamond implanted with 4-MeV carbon at $-196\,^{\circ}$C. Implantation at this high energy results in a damaged surface layer that looses long-range order, but retains a high degree of sp^3 bonding with some localized sp^2 bonding. This is reflected in the Raman spectra by a loss of the triply degenerate diamond peak at 1332 cm^{-1} and the appearance of a broad peak resembling the density of states of sp^3 amorphous carbon. Three additional and previously unreported peaks were observed above 1332 cm^{-1}. It is likely that these peaks reflect a mixture of sp^3 and sp^2 bonding in the implanted region. A small peak at 1451 cm^{-1} and a relatively sharp peak at 1498 cm^{-1} are present in a dose range of $10^{16}-10^{17}$ cm^{-2}. A third strong peak at 1634 cm^{-1} persists even to the maximum dose of 1.3×10^{18} cm^{-2}. Both the formation of the damage morphology retaining a high degree of sp^3 bonding and appearance of these peaks are unique to MeV energy implantation.

ACKNOWLEDGMENTS

This work is supported by the Division of Material Sciences, U.S. Department of Energy, under Contract No. DE-AC05-84OR21400 with Martin Marietta Energy Systems, Inc. and in part by an appointment to the Oak Ridge National Laboratory Postdoctoral Research Program administered by the Oak Ridge Institute for Science and Education.

[1]R. Shuker and R. W. Gammon, Phys. Rev. Lett. **25**, 222 (1970).
[2]J. E. Smith, Jr., M. H. Brodsky, B. L. Crowder, and M. I. Nathan, J. Non-Cryst. Solids **8–10**, 179 (1972).
[3]N. Maley and J. S. Lannin, Phys. Rev. B **35**, 2456 (1987).
[4]Fang Li and Jeffrey S. Lannin, Phys. Rev. B **39**, 6220 (1989).
[5]D. Beeman, J. Silverman, R. Lynds, and M. R. Anderson, Phys. Rev. B **30**, 870 (1984).
[6]C. Z. Wang and K. M. Ho, Phys. Rev. Lett. **71**, 1184 (1993).
[7]N. Wada, P. J. Gaczi, and S. A. Solin, J. Non-Cryst. Solids **35-36**, 543 (1980).
[8]W. S. Bacsa, J. S. Lannin, D. L. Pappas, and J. J. Cuomo, Phys. Rev. B **47**, 10 931 (1993).
[9]S. Sato, H. Watanabe, K. Takahashi, Y. Abe, and M. Iwaki, Nucl. Instrum. Methods Phys. Res. Sect. B **59/60**, 1391 (1991).
[10]E. H. Lee, D. M. Hembree, Jr., G. R. Rao, and L. K. Mansur,

Phys. Rev. B **48**, 15 540 (1993).
[11]J. Lindhard, M. Scharff, and H. E. Schiott, Mat. Fys. Medd. Dan. Vid. Selsk. **33** (14) (1963).
[12]J. F. Ziegler, J. P. Biersack, and U. Littmark, *The Stopping and Range of Ions in Solids* (Pergamon, New York, 1985).
[13]N. R. Parikh, J. D. Hunn, E. McGucken, M. L. Swanson, C. W. White, R. A. Rudder, D. P. Malta, J. B. Posthill, and R. J. Markunas, Appl. Phys. Lett. **61**, 3124 (1992).
[14]J. Walker, Rep. Prog. Phys. **42**, 1605 (1979).
[15]J. D. Hunn, S. P. Withrow, R. E. Clausing, L. Heatherly, J. Bentley, D. M. Hembree Jr., and N. R. Parikh, in *Materials Synthesis and Processing Using Ion Beams,* edited by R. J. Culbertson, K. S. Jones, O. W. Holland, and K. Maex, MRS Symposia Proceedings No. 316 (Materials Research Society, Pittsburgh, 1994), p. 45.
[16]M. Posselt, Radiat. Eff. Defects Solids **130/131**, 87 (1994).
[17]M. V. Klein, in *Light Scattering in Solids,* edited by M. Cardona, Topics in Applied Physics Vol. 8 (Springer, New York, 1975), pp. 147–204.
[18]N. Wada and S. A. Solin, Physica **105B**, 353 (1981).
[19]G. S. Sandhu, B. Liu, N. R. Parikh, J. D. Hunn, Th. Wichert, M. Deicher, H. Skudlik, W. N. Lennard, and I. V. Mitchell, in *Diamond, Silicon Carbide and Related Wide Bandgap Semiconductors,* edited by J. T. Glass, R. F. Messier, and N. Fujimori, MRS Symposia Proceedings No. 162 (Materials Research Soceity, Pittsburgh, 1990), p. 189.